Single-Atom Catalysts

Deutsche Ausgabe: DOI: 10.1002/ange.201608597
Internationale Ausgabe: DOI: 10.1002/anie.201608597

Efficient Visible-Light-Driven Carbon Dioxide Reduction by a Single-Atom Implanted Metal–Organic Framework

*Huabin Zhang, Jing Wei, Juncai Dong, Guigao Liu, Li Shi, Pengfei An, Guixia Zhao, Jintao Kong, Xiaojun Wang, Xianguang Meng, Jing Zhang, and Jinhua Ye**

Abstract: *Modular optimization of metal–organic frameworks (MOFs) was realized by incorporation of coordinatively unsaturated single atoms in a MOF matrix. The newly developed MOF can selectively capture and photoreduce CO_2 with high efficiency under visible-light irradiation. Mechanistic investigation reveals that the presence of single Co atoms in the MOF can greatly boost the electron–hole separation efficiency in porphyrin units. Directional migration of photogenerated excitons from porphyrin to catalytic Co centers was witnessed, thereby achieving supply of long-lived electrons for the reduction of CO_2 molecules adsorbed on Co centers. As a direct result, porphyrin MOF comprising atomically dispersed catalytic centers exhibits significantly enhanced photocatalytic conversion of CO_2, which is equivalent to a 3.13-fold improvement in CO evolution rate ($200.6\,\mu mol\,g^{-1}\,h^{-1}$) and a 5.93-fold enhancement in CH_4 generation rate ($36.67\,\mu mol\,g^{-1}\,h^{-1}$) compared to the parent MOF.*

Atomically dispersed catalysts comprising mononuclear metal complexes or single metal atoms anchored on supports offer maximum atom efficiency and provide the most ideal strategy to create highly efficient catalysts.[1] Moreover, catalysts with atomically dispersed active sites are model systems that allow understanding of heterogeneous catalysis at the molecular level, bridging the gap between heterogeneous and homogeneous catalysis. However, fabrication of practical and stable single-atom catalysts remains a significant challenge because, single atoms are typically too mobile and easy to sinter under realistic reaction conditions.[2] MOFs—a class of porous and crystalline materials—provide the most effective coordination sites to anchor individual metal atoms, thereby preventing sintering during catalysis.[3]

Global energy demands and climate change underpin broad interest in the sustainable reduction of CO_2 into value-added carbon products, such as CO and hydrocarbon fuels. Photocatalytic reduction of CO_2 is a highly important route for solar-to-chemical energy conversion by mimicking the natural photosynthetic process.[4] A great deal of effort has been devoted to exploring photocatalysts that are capable of capturing and reducing CO_2. However, the photocatalytic efficiency of currently developed catalysts is far from satisfactory, largely because of low specific surface area, confined active sites, and fast recombination of the photogenerated electron–hole pairs.[5] Photocatalysts are excited by light absorption to generate electron–hole pairs that are then separated and transferred to different sites for redox reactions. The separation efficiency of the photoinduced charge carriers and the highly directional transfer of excitons, play an important role in the final catalytic activity.[6] Increasing the CO_2 adsorption ability of photocatalysts is an effective strategy to improve CO_2 conversion efficiency, as electron transfer from the catalytically active sites of the photocatalysts to CO_2 largely relies on intimate and stable binding interactions with CO_2 molecules. Nevertheless, investigation of photocatalytic CO_2 reduction using MOFs or MOF-based composites is still at an early stage. Low charge separation and energy transfer efficiency, as well as inconsistencies between catalytic and adsorption sites, are main drawbacks to visible-light-driven CO_2 reduction.[7]

Bearing these aspects in mind, and motivated by the fact that exciton migration in natural photosynthesis primarily occurs in highly ordered porphyrin-like pigments, we considered that equally ordered porphyrin-based MOFs might exhibit similar behavior, thereby facilitating antenna-like light-harvesting, and positioning such materials for use in solar energy conversion schemes.[8] MOF-525, formulated as $Zr_6O_4(OH)_4(TCPP\text{-}H_2)_3$ [TCPP = 4,4′,4″,4‴-(porphyrin-5,10,15,20-tetrayl) tetrabenzoate], which integrates Zr_6 clusters and porphyrin-based molecular units into a 3D network, was selected as a MOF matrix for its excellent performance in CO_2 capture and visible-light utilization.[8a] Coordinatively unsaturated Co sites were incorporated into the porphyrin units to generate a new composite, MOF-525-Co, in which each active site is guaranteed simultaneous exposure to molecular CO_2 and can avoid aggregation of active sites (Figure 1 a; Supporting Information, Figure S1). Introduction

[*] Dr. H. Zhang, Dr. G. Liu, L. Shi, Dr. G. Zhao, Dr. X. Wang, Dr. X. Meng, Prof. J. Ye
International Center for Materials Nanoarchitectonics (WPI-MANA)
National Institute for Materials Science (NIMS)
1-1 Namiki, Tsukuba, Ibaraki 305-0044 (Japan)
E-mail: Jinhua.YE@nims.go.jp
Prof. J. Ye
TU-NIMS Joint Research Center, School of Material Science and Engineering, Tianjin University, Tianjin 300072 (P.R. China)
and
Collaborative Innovation Center of Chemical Science and Engineering (Tianjin), Tianjin 300072 (P.R. China)
Dr. J. Wei, Dr. J. Kong
Fujian Institute of Research on the Structure of Matter
Chinese Academy of Sciences
Fuzhou 350002 (P.R. China)
Dr. J. Dong, Dr. P. An, Prof. J. Zhang
Beijing Synchrotron Radiation Facility, Institute of High Energy Physics, Chinese Academy of Sciences
Beijing 100049 (P.R. China)

Supporting information for this article can be found under: http://dx.doi.org/10.1002/anie.201608597.

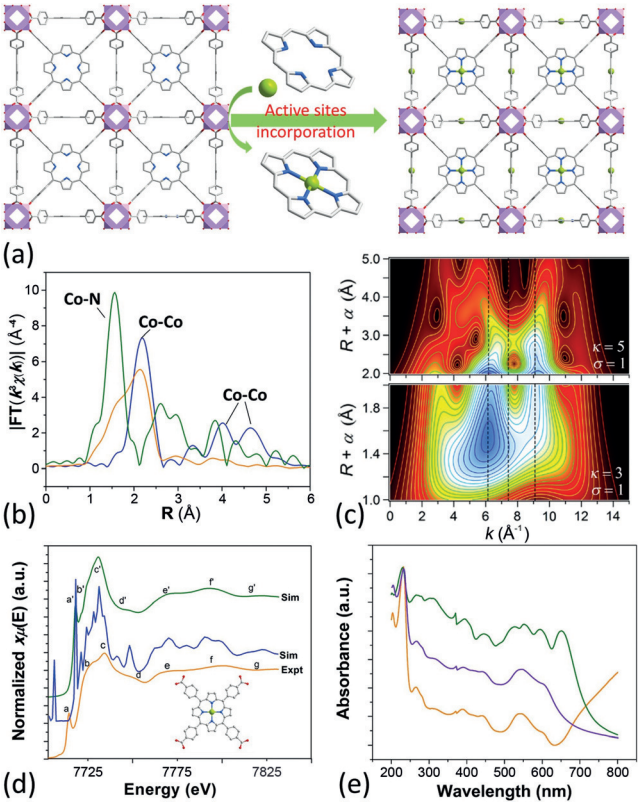

Figure 1. a) View of the 3D network of MOF-525-Co featuring a highly porous framework and incorporated active sites. b) Fourier transform magnitudes of the experimental Co *K*-edge EXAFS spectra of samples (not corrected for phase shift). Key: Co foil (blue), Co@C (orange), MOF-525-Co (green). c) Wavelet transform for the k^3-weighted EXAFS signal of MOF-525-Co, based on Morlet wavelets with optimum resolution at the first (lower panel) and higher (upper panel) coordination shells. Vertical dashed lines denoting the *k*-space positions of the Co-N and Co-Co contributions are provided to guide the eye. d) Comparison between the Co K-edge XANES experimental spectrum (orange) of MOF-525-Co and the theoretical spectrum calculated with the depicted structure. For clarity, the non-convoluted theoretical spectrum is also shown. e) UV/Vis spectra of MOF-525 (green), MOF-525-Co (purple), and MOF-525-Zn (orange).

of unsaturated Co sites generates efficient catalytically active sites and also enhances CO_2 adsorption over the open sites of Co porphyrins, thus realizing the activation of molecular CO_2.[8c] Furthermore, directional energy migration within the MOF is greatly facilitated with the introduction of Co sites, which substantially suppress electron–hole recombination in the MOF, and supply long-lived electrons for the reduction of CO_2 molecules adsorbed on the MOF.[8]

Successful synthesis of MOF-525-Co was confirmed by the XRD pattern collected at room temperature, as well as by the color change of the samples (Supporting Information, Figures S2 and S3). To confirm the local coordination environment of the Co atom upon insertion within the framework, the Co K-edge extended X-ray absorption fine structure (EXAFS) and X-ray absorption near-edge structure (XANES) spectroscopies were investigated.[9] The EXAFS Fourier transforms (FTs) and wavelet transforms (WTs) are shown in Figure 1 b,c. Assignment of the signals from 1.0 to 5.0 Å to either Co-N(C) or Co-Co interactions is based on a detailed WT-EXAFS wavelet transform analysis (Supporting Information, Figures S4 and S5). For MOF-525-Co, a WT intensity maximum near 6.0 $Å^{-1}$ associated with a shoulder around 9.0 $Å^{-1}$ is well-resolved at 1.0–5.0 Å (Figure 1 c); this can be assigned to the Co–N bond. In comparison, a WT intensity maximum at 7.5 $Å^{-1}$ corresponding to the Co–Co bond is not detected in MOF-525-Co, indicating that almost all Co atoms exists as mononuclear centers.[10] EXAFS curve fitting analysis reveals that the coordination number of the nearest-neighbor N atoms surrounding the isolated Co atom is 3.9 at 1.95 Å (Supporting Information, Figure S5 and Table S1), further confirming the square-planar configuration of Co in the newly developed MOF and the presence of unsaturated active sites for catalytic reaction (Supporting Information, Figure S6 and Table S1). The high sensitivity of the 3D arrangement of atoms around the photoabsorber required application of XANES to better identify the newly developed MOF. Figure S7 (Supporting Information) reveals that the overall profile of the Co *K*-edge XANES spectrum of MOF-525-Co is drastically different from that of metallic Co, which suggests the existence of Co-N species. The square-planar configuration of a Co center with high D_{4h} symmetry was further qualitatively confirmed by the strong characteristic pre-edge peak at 7715 eV arising from a $1s \rightarrow 4p_z$ shake-down transition.[10] Moreover, we carried out XANES simulation of the CoN_xC_y moiety, which was built by situating a Co atom at the center of a porphyrinic unit within the crystal structure obtained by XRD Rietveld refinement. As shown in Figure 1 d, the seven features (denoted a–g) of the experimental XANES spectrum for MOF-525-Co are all satisfactorily reproduced, thus fully corroborating the unsaturated nature of single atoms implanted in MOF-525-Co.

Metallization of Zn in the MOF (MOF-525-Zn) was developed as a reference compound by a similar strategy. UV/Vis spectra indicated that MOF-525, MOF-525-Co, and MOF-525-Zn, were excellent photon absorbers from 200 to 800 nm (Figure 1 e). MOF-525 displays a strong S band and four Q bands, which are characteristic for the porphyrin family (Supporting Information, Figure S8). After metalation of the porphyrin ring with Co and Zn, the four Q bands become two because of the higher symmetry of the porphyrin unit in MOF-525-Zn and MOF-525-Co.[11] These results, combined with the Fourier transform infrared spectroscopy (FTIR) and inductively coupled plasma (ICP) elemental analysis, confirmed the successful incorporation of Zn and Co into the framework (Supporting Information, Table S2, Figures S9 and S12). These facts were further supported by XPS survey spectra; the free base porphyrin in MOF-525 contains two chemically different types of nitrogen atoms, (=*N*– and –NH), while MOF-525-Zn and MOF-525-Co produced single signals for Co–N or Zn–N bonding, respectively, in the asymmetric N 1s XPS spectra (Supporting Information, Figure S10).[11] Signals in the Co 2p and Zn 2p XPS spectra also indicated the introduction of these components into the framework (Supporting Information, Figure S11).

To elucidate the effect of metallization over porphyrin-based MOF, the catalytic behaviors of MOF-525-Co and

MOF-525-Zn were examined in the photochemical reduction of CO_2 and compared with that of MOF-525 (Supporting Information, Figure S13). The reduction proceeded upon irradiation with visible light, using triethanolamine (TEOA) as an electron donor, giving the two-electron reduction product CO together with the eight-electron reduction product CH_4 (Supporting Information, Figures S14–S17). As shown in Figure 2 a,b, the generation of CO and CH_4

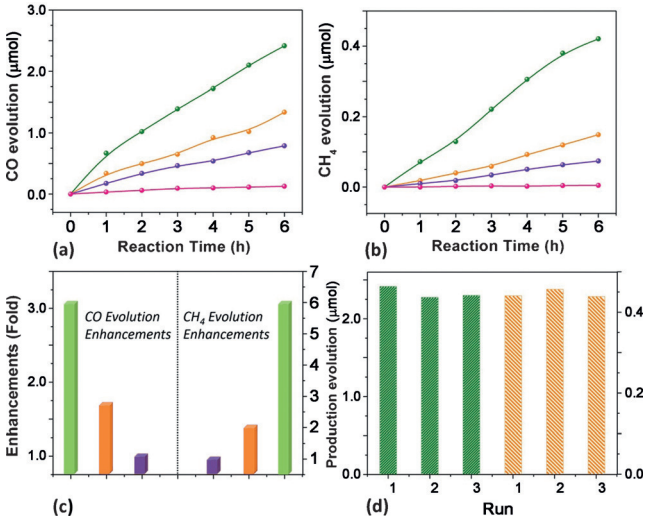

Figure 2. Time dependent a) CO and b) CH_4 evolution over MOF-525-Co (green), MOF-525-Zn (orange), MOF-525 (purple) photocatalysts, and H_6TCPP ligand (pink). c) Enhancement of production evolution over MOF-525-Co (green), MOF-525-Zn (orange), and MOF-525-Zn (purple). d) Production yield of CO (green) and CH_4 (orange) over MOF-525-Co photocatalyst as a measure of reproducibility by cycling.

increased almost linearly with irradiation time. MOF-525-Co composite showed the highest CO evolution rate of 200.6 $\mu mol\,g^{-1}\,h^{-1}$ (yield: 2.42 μmol), and a CH_4 evolution rate of 36.76 $\mu mol\,g^{-1}\,h^{-1}$ (yield: 0.42 μmol) under light illumination for 6 hours; much higher than that of MOF-525-Zn (CO, 111.7 $\mu mol\,g^{-1}\,h^{-1}$; CH_4, 11.635 $\mu mol\,g^{-1}\,h^{-1}$) and MOF-525 (CO, 64.02 $\mu mol\,g^{-1}\,h^{-1}$; CH_4, 6.2 $\mu mol\,g^{-1}\,h^{-1}$; Supporting Information, Table S3). These results also reveal that MOF-525-Co is an active catalyst for CO_2 reduction and is comparable with previously reported catalysts under similar conditions (Supporting Information, Table S5).[12] As demonstrated, superior efficiency in CO_2 conversion was realized by incorporation of unsaturated single atoms into Zr-porphyrin MOF: 1) CO_2 conversion enhancement is more obvious over MOF-525-Co than that of MOF-525-Zn; 2) compared with MOF-525, MOF-525-Co displayed 3.13-fold higher photocatalytic activity for CO evolution (two-electron reduction product) and meanwhile produced a 5.93-fold enhancement in CH_4 evolution (eight-electron reduction product), which clearly confirmed that the selectivity of CH_4 was significantly improved by metallization of Co (Figure 2 c).

Additionally, MOF-525-Co exhibits excellent performance stability in recycling tests, and produced a fairly reproducible photocatalytic activity for all three cycles. When the experiment was conducted in the absence of photocatalysts or light illumination, no detectable products were formed in the reaction system (Supporting Information, Figure S21). To further validate the source of the generated CO and CH_4 products, an isotopic experiment using $^{13}CO_2$ as substrate was performed under identical photocatalytic reaction conditions, and the products were analyzed by gas chromatography and mass spectra. As shown in Figure S22 (Supporting Information), the peak at $m/Z = 29$ and $m/Z = 17$ could be assigned to ^{13}CO and $^{13}CH_4$, respectively, indicating that the carbon source of CO and CH_4 does indeed originate from the CO_2 used.

Consequently, we are in a position to understand the mechanisms behind the function of the newly developed structures. CO_2 adsorption is of vital importance to the final catalytic result. Volumetric CO_2 adsorption measurement reveals increased uptakes after metallization at all pressures up to 100 kPa (Figure 3 a; Supporting Information, Table S3).

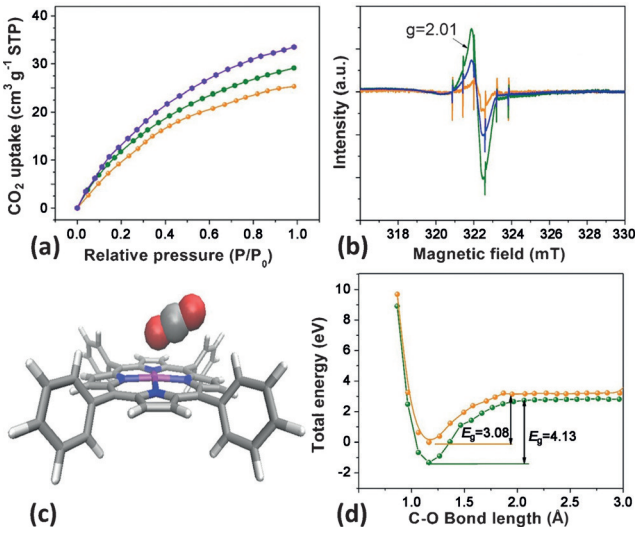

Figure 3. a) CO_2 adsorption behaviors for MOF-525 (orange) as well as MOF-525-Co (purple) and MOF-525-Zn (green) implanted with single atoms. b) ESR spectra of MOF-525-Co under different conditions. Key: light and N_2 (orange), light and CO_2 (purple), N_2 (green). c) The optimized structure for CO_2 adsorption on a porphyrin–Co unit. d) The O—C bond length-dependent CO_2 activation energy barrier. Key: charged with one electron (orange), neutral state (green).

These results can be interpreted in terms of increase in the affinity sites for adsorbates after metallization, which should partly account for the enhanced catalytic capability observed. In situ FTIR technology is a crucial tool for investigation of the local interactions between the active sites and molecular CO_2, in which the asymmetric stretching mode of CO_2 ($\nu_3 = 2349\ cm^{-1}$) is infrared active and thus serves as a handle for identifying the nature of the adsorption behavior. As shown in Figure S23 (Supporting Information), infrared spectra collected from a blank sample in a CO_2 atmosphere exhibit a strong peak centered at 2334 cm^{-1}, which is attributed to the ν_3 band of CO_2.[13] In the case of MOF-525-Co, the adsorption of CO_2 onto the exposed Co^{II} adsorption sites resulted in a 31 cm^{-1} red shift of the ν_3 band because of the electron donation from the oxygen lone pairs on CO_2 to the

unoccupied Co^{II} orbitals. The enhanced CO_2 adsorption activity over MOF-525-Co and MOF-525-Zn, as well as the in situ FTIR spectra, reveal the strong interaction between molecular CO_2 and adsorption sites, and also demonstrate the integration of the active centers and reagents adsorption sites. Therefore, enhanced CO_2 reduction activity can be guaranteed with the implantation of metal ions in the porphyrin moiety.

Taking into account that MOF-525-Co and MOF-525-Zn have similar surface area and CO_2 adsorption ability, the significant difference in the activity enhancement for the two catalysts should be partially ascribed to the difference in charge separation efficiencies as a function of donor–acceptor interaction (Supporting Information, Figure S12). Porphyrin-containing struts are the primary building blocks used in MOFs that target solar light harvesting. These porphyrin units are proven to have exciton propagation capabilities, displaying anisotropic energy transport over several tens of struts from the initially excited strut.[8] Instantaneous electron transfer from the porphyrin moiety to the reaction centers can be monitored by incident-photon-to-current conversion efficiency (IPCE) characterization. The transient photocurrents of the samples were examined during light ON–OFF cycling at 0.6 V (vs. NHE) as shown in Figure S24 (Supporting Information). Enhanced efficiency in separating the photogenerated electron–hole pairs over MOF-525-Co and MOF-525-Zn is attributed to the energy transfer from porphyrin units to a lower energy Co or Zn "trap site". Notably, the current intensity of MOF-525-Co is much higher than that for MOF 525-Zn, which partially accounts for the difference in catalytic activity over these two samples.

Further insight into the electron transfer behavior was gained by photoluminescent (PL) quenching experiments. With incorporation of metal ions into the porphyrin ring, significant quenching of the PL intensities of the porphyrin emission was observed—especially for porphyrin-Co units—indicating that the recombination of photoexcited electron–hole pairs is significantly suppressed and the separation of electron–hole pairs is efficiently improved (Supporting Information, Figure S25). Time-resolved decays for MOF-525-Co and MOF-525-Zn implanted with metal sites demonstrated more rapid decay than unmodified MOF-525 (Supporting Information, Figure S26). Analysis of the curves with a reconvolution fit supported a triexponential decay model in each case and revealed a shortening of the amplitude-weighted average lifetimes from 90.25 (MOF-525) to 68.35 and 34.15 ns in the presence of the acceptor molecules in MOF-525-Zn and MOF-525-Co, respectively (Supporting Information, Table S4). To quantitatively describe the energy transfer (ET) processes occurring in the photocatalytic process, we sought an independent measurement of the ET efficiency (Φ_{ET}) based on the time-resolved fluorescence decay lifetimes (Supporting Information, Equation S1).[14] The Φ_{ET} was determined based on donor lifetimes in the presence and absence of the acceptor molecules. Compared with MOF-525-Zn ($\Phi_{ET} = 24.9\,\%$), a relatively larger Φ_{ET} ($\Phi_{ET} = 62.1\,\%$) was observed for MOF-525-Co, which could further account for the more enhanced catalytic activity in MOF-525-Co (Supporting Information, Table S3). Thus, directional migration of photogenerated excitons from porphyrin to electron trapping sites was realized by the implantation of catalytic Co single atoms, achieving supply of long-lived electrons for the reduction of CO_2 molecules adsorbed on Co centers.

After clarifying the charge transfer route from the excited porphyrin to the reaction centers, we turned our attention to the reaction kinetics over the activation sites. ESR spectroscopy can provide valuable fingerprinting information about trapped electrons and interface states in reaction process. For MOF-525, a *g* value of 1.9984 was observed at room temperature under nitrogen gas atmosphere, which could be ascribed to the free radicals produced by the porphyrin-based ligand.[15a] With light irradiation, an enhanced ESR signal with a *g* value of 1.9984 and a new ESR signal with a *g* value of 2.0048 were observed, which provided a clue about the promoted photogeneration of radical pairs in MOF-525 and the subsequent charge transfer process (Supporting Information, Figure S27). According to the literature, the new signal can be attributed to Zr^{III} species formed from the optically induced hopping of electrons from Zr^{IV} to Zr^{III} sites in the Zr oxo-clusters.[15b] These studies conclusively demonstrate charge transfer from porphyrin ligand to Zr oxo-clusters, without the insertion of additional sites in the MOF matrix. However, in the case of the MOF-525-Co composite without irradiation, a strong signal for high-spin state Co^{II} was observed, accompanied by a signal from the porphyrin unit (Figure 3b). With visible-light irradiation, the peak intensity of Co^{II} was greatly weakened, which clearly indicates an optically induced valence transformation from high-spin state Co^{II} to Co^{I} in a low-spin state.[15c] When CO_2 was introduced into the irradiated MOF-525-Co system, the ESR signal corresponding to Co^{II} was enhanced, implying that some of the Co^{I} was oxidized back to Co^{II} species during the CO_2 photoreduction process.[12c] This kinetic behavior also indicates that photoexcited electrons are transferred to the Co center, thereby realizing valence transformation of the Co center. It is rather interesting that the Zr^{III} signal in MOF-525-Co nearly disappeared under light irradiation. We tentatively draw the conclusion that the coordination between the porphyrin ring and Co center most likely leads to effective shuttering of the electron-transfer channels from the porphyrin units to Zr oxo-clusters.

The improved efficiency of charge separation in our designed hybrid system was clearly demonstrated in the above discussion (Supporting Information, Figure S28). A theoretical model was constructed to simulate the reaction process and examine whether CO_2 molecules can be activated well on the coordinately unsaturated Co sites of the MOFs upon acquisition of photoexcited electrons from the porphyrin unit (Figure 3c). The activation of CO_2 molecules is attributed to a high concentration of localized electrons in the near-surface region and a corrugation of the surface that can trap oxygen atoms from CO and CO_2 molecules. First-principles simulations reveal that the addition of electron charges can greatly improve adsorption of CO_2 to the active sites, resulting in a calculated adsorption energy increase from 0.865 to 2.189 eV. The simulated potential energy surfaces, corresponding to variation of the O–C bond of the CO_2 molecules adsorbed on active sites, are plotted in Figure 3d.

The addition of a one-electron charge barely alters the activation-energy barrier (EB) for CO_2, and substantially lowers the EB from 4.13 to 3.08 eV. These results clearly indicate that upon acquisition of photoexcited electrons from porphyrin units, the coordinatively unsaturated Co centers become an active catalytic material for the activation of CO_2 molecules.

In conclusion, we realized atomic dispersion of active sites in an extended MOF, thus generating photocatalysts with higher activity in CO_2 reduction. Unique structural characteristics of the developed catalyst include a large surface area and strong CO_2 adsorption ability. As demonstrated by an energy transfer efficiency investigation, as well as first-principles simulations, photogenerated electrons can be effectively transferred to the active sites, which not only facilitates charge separation in the semiconducting MOF but also supplies energetic electrons to gas molecules adsorbed on the MOF. After incorporation of active sites, CO_2 can be easily captured and subsequently photocatalytically reduced into CO and CH_4 with dramatically improved performance in terms of both activity and CH_4 selectivity. We anticipate that this implantation strategy, combined with molecular material platforms, will be applicable to a broad range of catalytic applications; particularly those that require solar harvesting and gaseous compatibility.

Acknowledgements

This research received financial support from the World Premier International Research Center Initiative (WPI Initiative) on Materials Nanoarchitectonics (MANA), MEXT (Japan), and the National Basic Research Program of China (973 Program, 2014CB239301 and NSFC11605225). J.D. acknowledges support from the Jianlin Xie Foundation of the Institute of High Energy Physics, Chinese Academy of Sciences.

Keywords: active sites · CO_2 reduction · heterogeneous catalysis · photocatalysis · solar-energy conversion

How to cite: *Angew. Chem. Int. Ed.* **2016**, *55*, 14310–14314
Angew. Chem. **2016**, *128*, 14522–14526

[1] a) J. Lin, A. Wang, B. Qiao, X. Liu, X. Yang, X. Wang, J. Liang, J. Li, J, Liu, T. Zhang, *J. Am. Chem. Soc.* **2013**, *135*, 15314–15317; b) P. Liu, Y. Zhao, R. Qin, S. Mo, G. Chen, D. M. Chevrier, P. Zhang, Q. Guo, D. Zang, B. Wu, G. Fu, N. Zheng, *Science* **2016**, *352*, 797–801.

[2] a) Y. Lei, F. Mehmood, S. Lee, J. Greeley, B. Lee, S. Seifert, R. E. Winans, J. W. Elam, M. J. Pellin, L. A. Curtiss, S. Vajda, *Science* **2010**, *328*, 224–228; b) C. Liu, B. Yang, E. Tyo, S. Seifert, J. DeBartolo, B. Issendorff, P. Zapol, S. Vajda, L. A. Curtiss, *J. Am. Chem. Soc.* **2015**, *137*, 8676–8679; c) F. Li, Y. Li, X. C. Zeng, Z. Chen, *ACS Catal.* **2015**, *5*, 544–552.

[3] a) K. Manna, T. Zhang, F. X. Greene, W. Lin, *J. Am. Chem. Soc.* **2015**, *137*, 2665–2673; b) H. Zhang, G. Liu, L. Shi, J. Tang, H. Pang, K. Wu, T. Takei, J. Zhang, Y. Yamauchi, J. Ye, *NPG Asia Mater.* **2016**, *8*, DOI: 10.1038/am.2016.102.

[4] a) H. Xu, J. Hu, D. Wang, Z. Li, Q. Zhang, Y. Luo, S.-H. Yu, H.-L. Jiang, *J. Am. Chem. Soc.* **2015**, *137*, 13440–13443; b) S. Wang, W. Yao, J. Lin, Z. Ding, X. Wang, *Angew. Chem. Int. Ed.* **2014**, *53*, 1034–1038; *Angew. Chem.* **2014**, *126*, 1052–1056; c) H. Zhang, T. Wang, J. Wang, T. D. Dao, M. Li, G. Liu, X. Meng, K. Chang, L. Shi, T. Nagao, J. Ye, *Adv. Mater.* **2016**, *28*, 3703–3710.

[5] a) L. Long, J. Chen, X. Zhang, A. Zhang, Y. Huang, Q. Rong, H. Yu, *NPG Asia Mater.* **2016**, *8*, DOI: 10.1038/am.2016.46; b) L. Duan, L. Wang, F. Li, L. Sun, *Acc. Chem. Res.* **2015**, *48*, 2084–2096.

[6] a) M. Yamamoto, L. Wang, F. Li, T. Fukushima, K. Tanaka, L. Sun, H, Imahori, *Chem. Sci.* **2016**, *7*, 1430–1439; b) H. Li, F. Li, B. Zhang, X. Zhou, F. Yu, L, Sun, *J. Am. Chem. Soc.* **2015**, *137*, 4332–4335.

[7] a) N. Kornienko, Y. Zhao, C. Zhu, D. Kim, S. Lin, C. Chang, O. M. Yaghi, P, Yang, *J. Am. Chem. Soc.* **2015**, *137*, 14129–14135; b) D. J. Darensbourg, W.-C. Chung, K. Wang, H.-C. Zhou, *ACS Catal.* **2014**, *4*, 1511–1515.

[8] a) W. Morris, P. L. McGrier, H. Furukawa, D. Cascio, J. F. Stoddart, O. M. Yaghi, *Inorg. Chem.* **2012**, *51*, 6443–6445; b) I. Hod, M. D. Sampson, P. Deria, O. K. Farha, J. T. Hupp, *ACS Catal.* **2015**, *5*, 6302–6309; c) J. A. Johnson, J. Luo, X. Zhang, Y.-S. Chen, M. D. Morton, E. Echeverría, F. E. Torres, J. Zhang, *ACS Catal.* **2015**, *5*, 5283–5291.

[9] D. C. Koningsberger in *X-ray absorption: principles, applications, techniques of EXAFS, SEXAFS, and XANES*, *Vol. 92* (Eds.: R. Prins), Wiley, New York, **1988**.

[10] a) H. Fei, J. Dong, M. J. A-Jimenez, G. Ye, N. D. Kim, E. L. G. Samuel, Z. Peng, Z. Zhu, F. Qin, J. Bao, M. J. Yacaman, P. M. Ajayan, D. Chen, J. M. Tour, *Nat. Commun.* **2015**, *6*, 8668; b) T. E. Westre, P. Kennepohl, J. G. DeWitt, B. Hedman, K. O. Hodgson, E. I. Solomon, *J. Am. Chem. Soc.* **1997**, *119*, 6297–6314.

[11] S. Afzal, W. A. Daoud, S. J. Langford, *ACS Appl. Mater. Interfaces* **2013**, *5*, 4753–4759.

[12] a) D. Wang, R. Huang, W. Liu, D. Sun, Z. Li, *ACS Catal.* **2014**, *4*, 4254–4260; b) Y. Lee, S. Kim, J. K. Kang, S. M. Cohen, *Chem. Commun.* **2015**, *51*, 5735–5738; c) Y. Fu, D. Sun, Y. Chen, R. Huang, Z. Ding, X. Fu, Z. Li, *Angew. Chem. Int. Ed.* **2012**, *51*, 3364–3367; *Angew. Chem.* **2012**, *124*, 3420–3423; d) H. Zhang, G. Liu, L. Shi, H. Liu, T. Wang, J. Ye, *Nano Energy* **2016**, *22*, 149–168; e) L. Shi, T. Wang, H. Zhang, K. Chang, J. Ye, *Adv. Funct. Mater.* **2015**, *25*, 5360–5367.

[13] J. A. Lercher, V. Veefkind, K. Fajerwerg, *Vib. Spectrosc.* **1999**, *19*, 107–121.

[14] J. R. Lakowicz, *Principles of Fluorescence Spectroscopy Principles of Fluorescence Spectroscopy*, Springer, Heidelberg, **2007**.

[15] a) D. Feng, H. Jiang, Y. Chen, Z. Gu, Z. Wei, H.-C. Zhou, *Inorg. Chem.* **2013**, *52*, 12661–12667; b) J. Long, S. Wang, Z. Ding, C. Wang, Y. Zhou, L. Huang, X. Wang, *Chem. Commun.* **2012**, *48*, 11656–11658; c) J. McAlpin, G. Surendranath, M. Dincă, T. A. Stich, S. A. Stoian, W. H. Casey, D. G. Nocera, R. D. Britt, *J. Am. Chem. Soc.* **2010**, *132*, 6882–6883.

Received: September 2, 2016
Published online: October 13, 2016

